Bioorganic & Medicinal Chemistry Letters 23 (2013) 5401–5409

Contents lists available at ScienceDirect

Bioorganic & Medicinal Chemistry Letters

journal homepage: www.elsevier.com/locate/bmcl

Fragment-based discovery of focal adhesion kinase inhibitors

Ulrich Grädler *, Jörg Bomke, Djordje Musil, Verena Dresing, Martin Lehmann, Günter Hölzemann, Hartmut Greiner, Christina Esdar, Mireille Krier, Timo Heinrich

Merck KGaA, Merck Serono Research, Frankfurter Str. 250, 64293 Darmstadt, Germany

ARTICLE INFO

Article history:
Received 26 April 2013
Revised 17 July 2013
Accepted 23 July 2013
Available online 31 July 2013

Keywords:
Fragment screening
Surface plasmon resonance
Focal adhesion kinase
X-ray structure
DFG-out

ABSTRACT

Chemically diverse fragment hits of focal adhesion kinase (FAK) were discovered by surface plasmon resonance (SPR) screening of our in-house fragment library. Site specific binding of the primary hits was confirmed in a competition setup using a high-affinity ATP-site inhibitor of FAK. Protein crystallography revealed the binding mode of 41 out of 48 selected fragment hits within the ATP-site. Structural comparison of the fragment binding modes with a DFG-out inhibitor of FAK initiated first synthetic follow-up optimization leading to improved binding affinity.

The nonreceptor tyrosine kinase FAK (EC 2.7.10.2) is composed by an N-terminal FERM domain (Four-point-one, ezrin, radixin, moesin), which regulates the enzymatic activity of its C-terminal kinase domain (KD).[1,2] Direct interaction of the FERM domain with the kinase C-lobe occludes the ATP-binding site and maintains an auto-inhibited conformation also by protecting the activation loop from phosphorylation by Src kinase. The auto-inhibitory state can be released upon interaction with FERM binding partners such as integrins and growth factors, underlining the important role of FAK in integrating diverse cellular signalling pathways. Disruption of the FERM–KD interaction leads to auto-phosphorylation of Tyr397 in the linker region and exposure of the activation loop. This is followed by binding of Src and phosphorylation of Tyr576 and Tyr577 within the FAK activation loop resulting in full catalytic activation of the enzyme.[3,4] Apart from playing a key role in regulation of normal cellular activities such as adhesion, migration and survival, FAK is also involved in cancer cell invasion, metastasis and survival. Therefore, FAK has been reported as attractive target for oncology and small molecule inhibitors are already in clinical phase-1 testing.[5–7]

Fragment-based lead discovery (FBLD) is considered as valuable technology within the pharmaceutical industry and has been reported to deliver lead series for a variety of drug targets.[8–10] FBLD uses a diverse library ($\sim 10^3$ molecules) of small molecules with MW typically below 250 Da for screening in contrast to high-throughput screening of large libraries ($\sim 10^6$ molecules). Fragments allow the sampling of a greater portion of chemical diversity and exploration of more binding motifs within the target. Even weak binding interactions of fragments to the protein target can be detected by applying high compound concentrations in biophysical methods such as NMR, surface plasmon resonance (SPR), or X-ray crystallography.[8–10]

In our FBLD campaign, we screened a library of 1920 fragments against the immobilized kinase domain of FAK using SPR (Fig. 1a).[11] Fragments were screened at a fixed concentration of 2 mM to remove 'sticky' and other bad behaving compounds.[12] At such high fragment concentrations, 80% of the fragments showed binding to the FAK surface. Therefore, the remaining fragments were tested again at 2 mM but in the presence of FAK-inhibitor **I** (Fig. 1b), which has been published by Roberts et al. at Pfizer (PF-562,271) as high-affinity ATP-competitive binder (IC_{50} = 1.5 nM).[13] The number of 'false-positive' hits (e.g., unspecific binders) could be dramatically decreased by using the FAK-inhibitor **I** for SPR competition experiments and fragments binding specifically within the ATP-pocket were identified. As a result, 180 fragments with a corresponding reduction in their binding levels in the presence of the competitor were selected as primary hits. The primary fragment hits were evaluated in further detail by SPR in titration series of 11 concentrations (1.95 μM to 2.0 mM). Steady state dissociation constants ($K_{D,ss}$) were determined by plotting the binding levels at the end of the association phase against the concentration (see Supplementary Fig. 3S for details) and then fitting the data to a single-site binding isotherm.

The affinity determination by SPR confirmed 105 hits with $K_{D,ss}$ values in the range of 13 μM to 3.5 mM, which were considered as

* Corresponding author. Tel.: +49 6151 725975; fax: +49 6151 72915975.
E-mail address: ulrich.graedler@merckgroup.com (U. Grädler).

0960-894X/$ - see front matter © 2013 Elsevier Ltd. All rights reserved.
http://dx.doi.org/10.1016/j.bmcl.2013.07.050

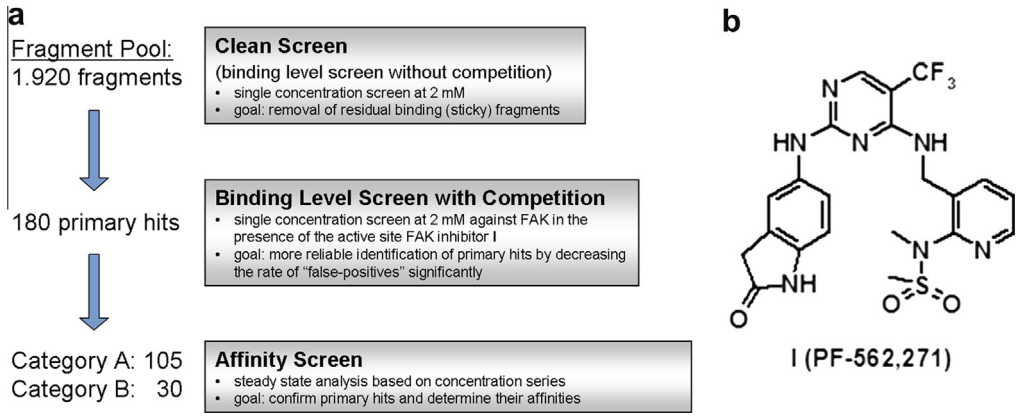

Figure 1. (a) FAK fragment screening strategy and results. (b) Structure of the FAK-inhibitor **I** (PF-562,271) used for SPR competition titration.

'category A' hits with highest confidence in binding.[14] In addition, 30 'category B' hits were discovered with the same characteristics as the 'category A' hits, but with limited compound solubility in DMSO or aqueous solution. We selected 48 'category A' and 2 'category B' hits by chemical diversity based on the Murcko framework representation and ligand efficiency (LE, range between 0.21 and

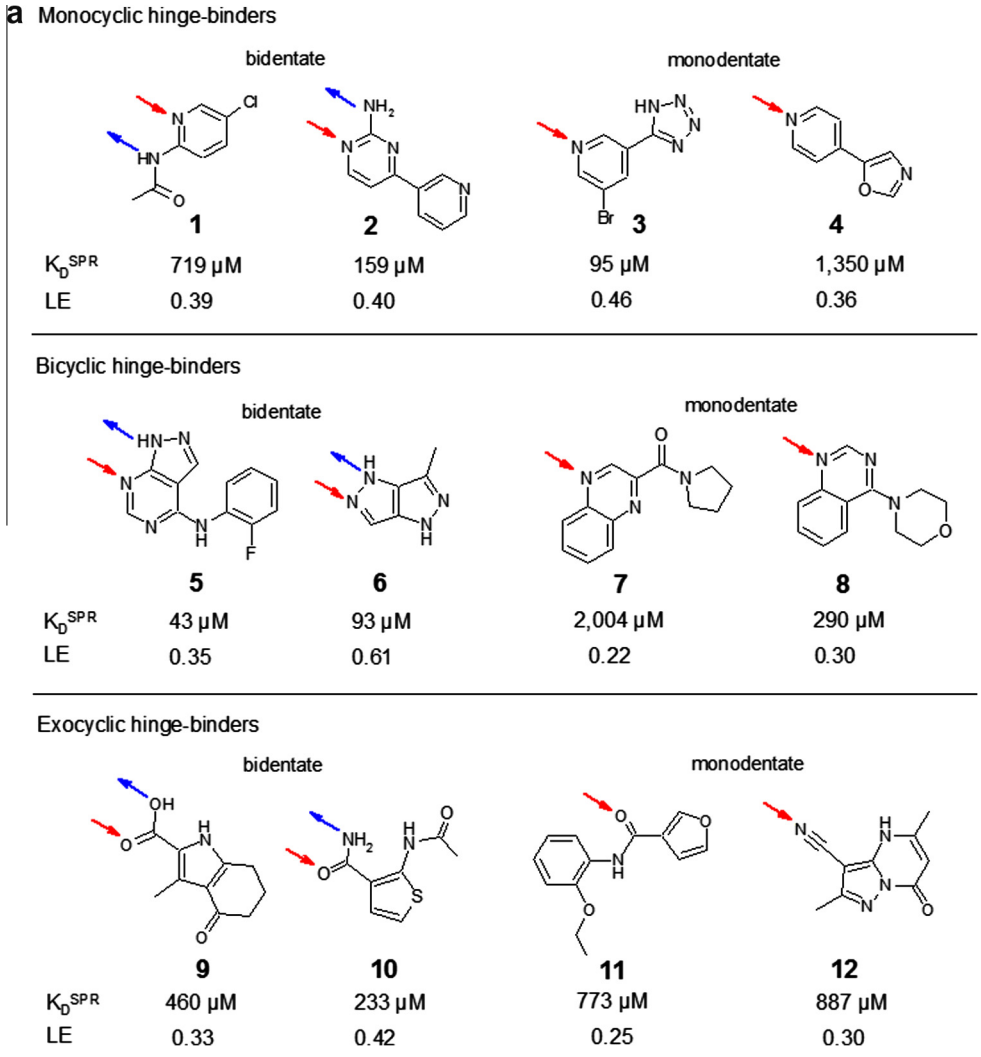

Figure 2. (a) Classification of representative FAK fragment-screening hits by the number of H-bond interactions (mono- and bidentate) to the hinge region (blue: donor contact, red: acceptor contact). (b) The X-ray structure of FAK in complex with fragment **6** at 2.7 Å resolution reveals alternative fragment binding orientations in the two monomers of the asymmetric unit (red: monomer A, green: monomer B). In both orientations, bi-dentate H-bond contacts (distances in Å) are formed to the hinge region (Glu500 and Cys502). The 2Fo–Fc electron density maps of the two binding modes are contoured at 1σ are shown in blue. (c) X-ray structure of FAK in complex with fragment **3** at 2.9 Å resolution (PDB ID: 4K8A) indicates one classical and two non-classical H-bonds (distances in Å) between the pyridine ring and the hinge region (Glu500 & Cys502). The 2Fo–Fc electron density map contoured at 1σ is shown in blue.

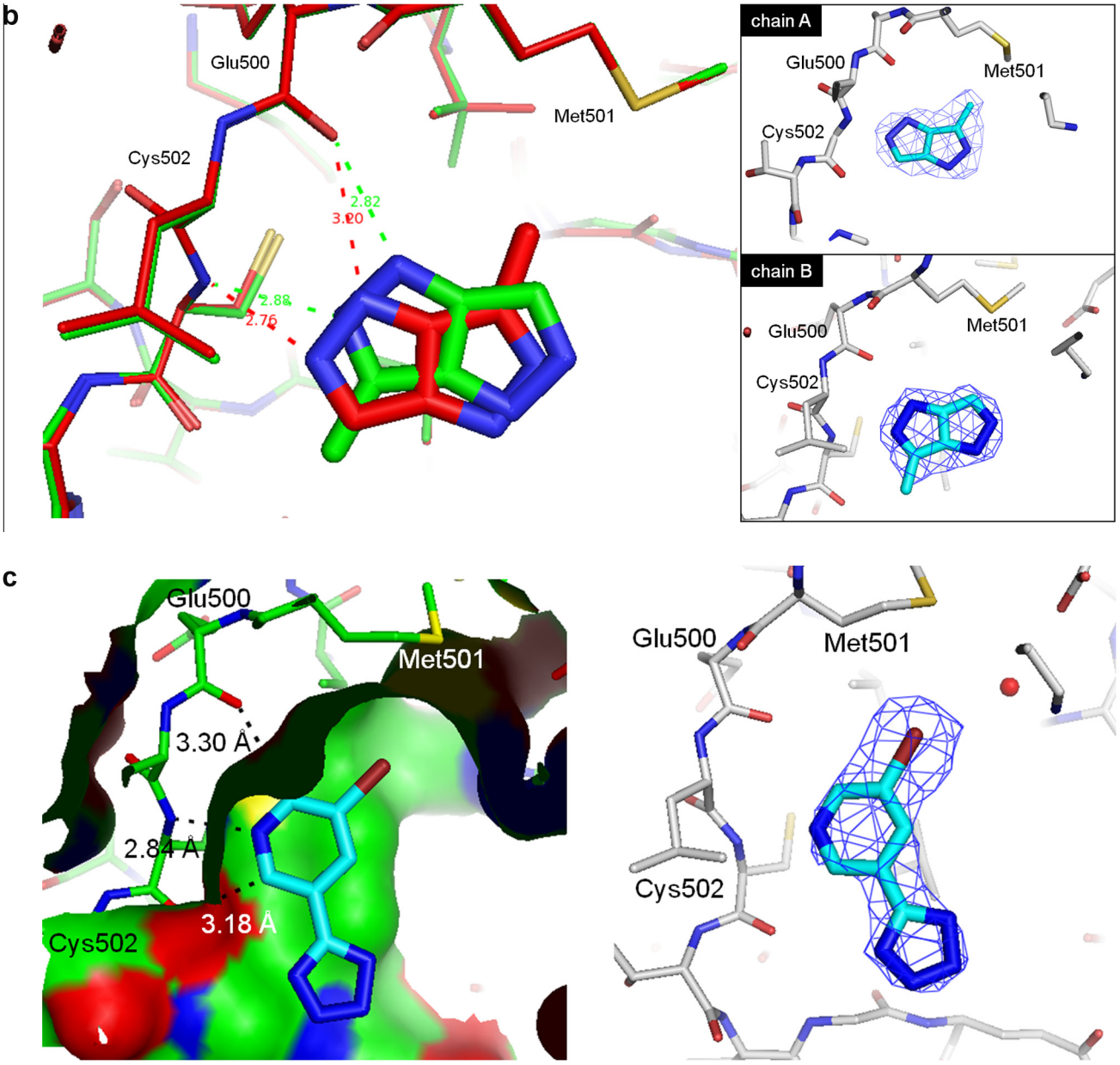

Fig. 2 (*continued*)

0.61) for protein crystallography using the kinase domain of FAK.[15,16] Our next goal was to determine as much protein-fragment structures as possible for a comprehensive exploration of binding interactions within the ATP-site of FAK. We therefore performed several soaking and co-crystallization experiments using saturating fragment concentrations of up to 10 mM.[17] In detail, we prepared 313 FAK crystals and successfully collected 121 datasets at the SLS synchrotron. Refinement of these datasets yielded 41 X-ray structures with clearly defined binding modes of the respective fragment within the ATP-site out of 48 selected 'category A' SPR hits, revealing a hit confirmation rate of 85%. The 41 X-ray structures were solved at resolutions between 2.0 and 2.9 Å and covered a fragment $K_{D,ss}$-range between 43 μM and 3.5 mM. However, for 9 fragments including the 2 'category B' hits ($K_{D,ss}$-range 13 μM–1.9 mM), difference electron densities in the ATP-site or other potential pockets were either ambiguous or not defined in multiple datasets (<3 Å) analyzed.

All 41 fragment hits validated by X-ray crystallography bound within the ATP-site of FAK and were classified based on the H-bond interaction pattern towards the hinge region (Fig. 2a). We observed mono- and bidentate H-bonds to the hinge region backbone amides of Glu500 and Cys502 formed by donor and acceptor groups within a variety of chemical scaffolds. Monocyclic hinge-binders such as 2-aminopyridine **1**, aminopyrimidine **2** or pyridines **3**–**4** as well as bicyclic scaffolds comprised in fragments **5**–**8** are well known interaction motifs in kinase inhibitors.[18] A fine balance of high ligand efficiency, synthetic feasibility and structure-based design yielded optimized inhibitors for many targets either by fragment growing, merging or linking.[19,20] In the present study, we focused our initial attempts of hit optimization on the fragments with the highest ligand efficiencies: **3** (LE = 0.46) and **6** (LE = 0.61). In the crystal structure of FAK in complex with pyrolo-pyrazole **6**, we observed two alternative fragment binding orientations in both monomers of the asymmetric unit (Fig. 2b, Supplementary Table S1).[21] In both orientations, bidentate H-bonds are formed between one of the pyrazole rings and the backbone amides of Glu500 and Cys502 of the hinge region. The binding modes of **6** are distinguished by the different orientation

of the methyl group in 3-position interacting with the gatekeeper residue Met501 or rotated by 180° towards Cys502 (Fig. 2b). A similar lipophilic interaction to Met501 is observed in the X-ray structure of FAK for the bromine atom of **3** (Fig. 2c, Supplementary Table S1). In the FAK·**3** structure, the fragment binding mode is identical in both monomers revealing the pyridine as monodentate hinge-binder (Fig. 2c).

The majority of reported protein kinase inhibitors bind ATP-competitive to the active kinase conformation (type I inhibitors) resulting in often limited kinase selectivity due to the high sequence conservation within the ATP-site. Targeting alternative conformations such as type II or type III characterized by a DFG-out conformation of the activation loop resulted in inhibitors with an improved selectivity profile.[22] Highly selective type III FAK inhibitors binding ATP non-competitively have been recently reported.[23] We previously described the structure-guided optimization of fragment hit **5** by merging with essential pharmacophores of the Pfizer-inhibitor **I** (PF-562,271) to target a unique helical activation-loop conformation of FAK.[24] A novel fragment merging opportunity became possible by our discovery of FAK inhibitor **13** with submicromolar potency (IC_{50}=266 nM, $K_{D,ss}$=111 nM) in a high-throughput screening campaign of FAK.[25] The crystal structure of FAK in complex with **13** was solved at 2.0 Å resolution and revealed a DFG-out conformation of the activation loop typical for type II inhibitor binding (Fig. 3a, Supplementary Table S1). Overall, the FAK·**13** structure is similar to the

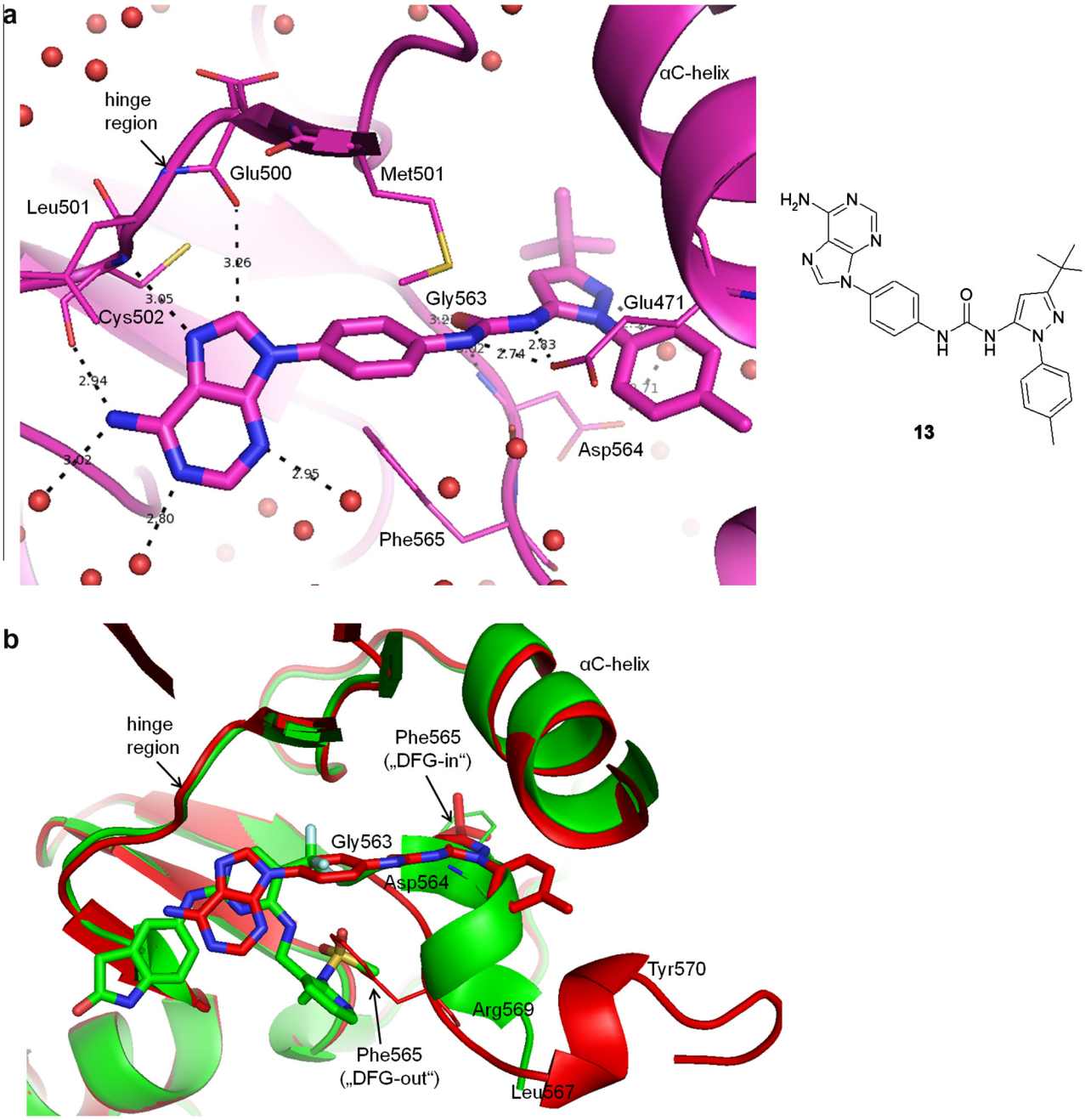

Figure 3. (a) The X-ray structure of human FAK in complex with **13** (PDB ID: 4K9Y) indicates a DFG-out conformation of Phe565 and specific H-bonds (dotted lines). (b) Comparison of FAK X-ray structures with the type II binder **13** (red) and the type I inhibitor **I** (PF-562,271; green; PDB ID: 3BZ3). The substituted pyrazole of **13** adopts the binding position of a short helical part of the activation loop including Phe565 of the DFG-motif. In the DFG-out conformation, Phe565 is shifted towards the ATP-site.

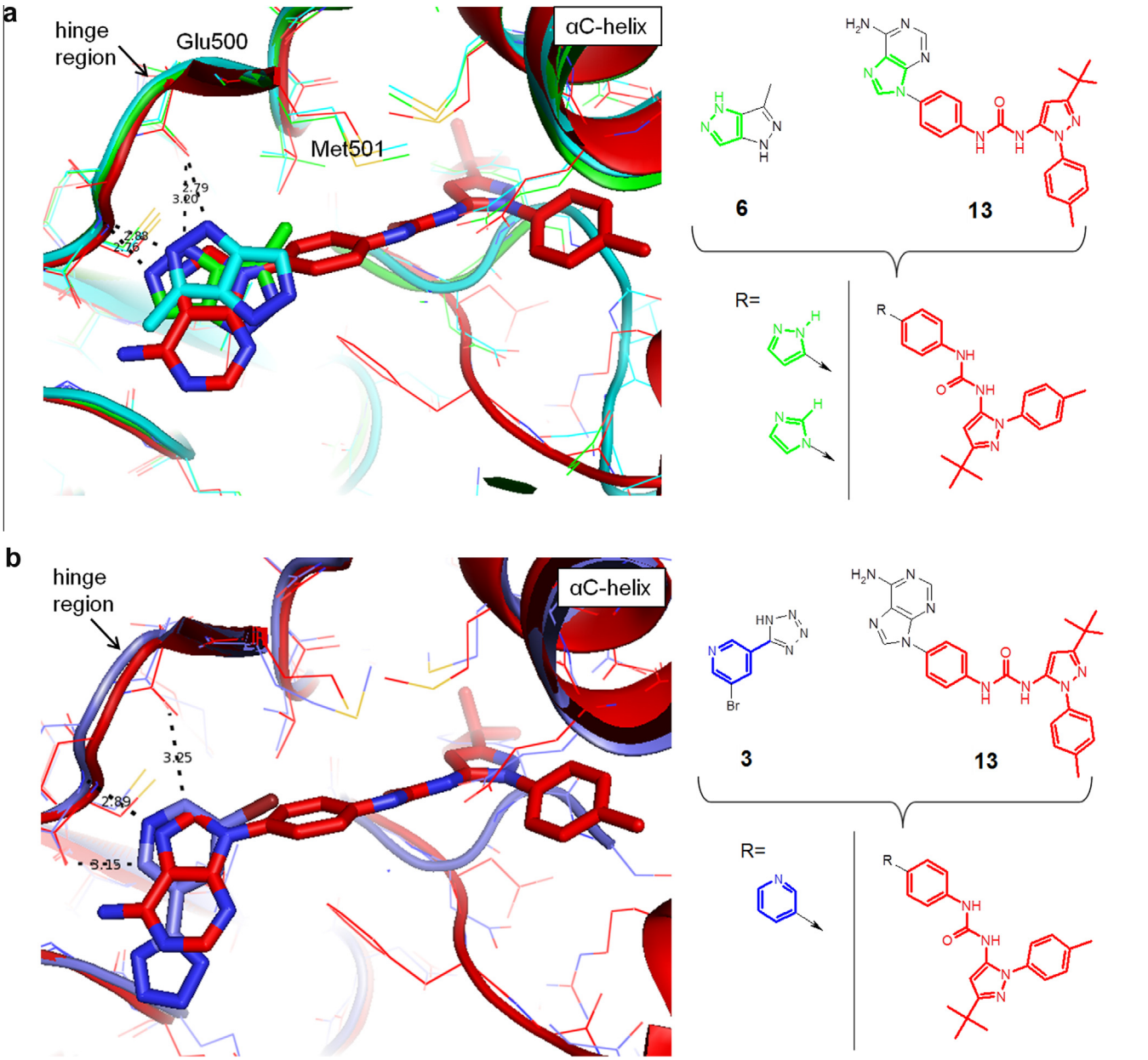

Figure 4. (a) Superimposition of FAK structures with type II binder **13** and fragment **6** indicates 5-membered rings (green) as purine replacements. Our design strategy included the diarylurea substituent of **13** (red) and 5-rings such as pyrazole or imidazole (green) bearing H-bond interactions to the hinge region. (b) Structural overlay of type II binder **13** and fragment **3** suggests 6-membered rings such as 3-pyridine (blue) as purine replacements. Our design strategy maintained the diarylurea substituent of **13** (red) in combination with 6-rings as hinge binders.

closely related proline-rich tyrosine kinase (PYK2) in complex with the diarylurea inhibitor PF-4618433 (PDB ID: 3BZ3, Supplementary Fig. 1S).[26] Indeed, **13** also inhibits PYK2 in a similar range (IC_{50} = 414 nM) as FAK underlining the high sequence identity of about 60% between the two kinases.[27] In FAK, the 5-*tert*-butyl-2-p-tolyl-pyrazole ring of **13** is buried into a lipophilic backpocket induced by conformational shift of Phe565 from the DFG-motif towards the ATP-site. Structural comparison with FAK·**I** demonstrates, that the substituted pyrazole ring of **13** partly adopts the binding position of the helical activation-loop involving residues Asp564 to Arg569 (Fig. 3b). This helical part is even shorter (Leu567-Tyr570) in the DFG-out structure and in van-der-Waals contact with the *p*-tolyl group of **13**. In the DFG-out position, Phe565 interacts via lipophilic contacts with the phenyl ring of **13**, which links the purine ring and the urea group attached to the pyrazole. The urea moiety of **13** forms H-bonds to Glu471 of the αC-helix and the backbone amide nitrogen of Gly563 preceding the DFG-motif. Surprisingly, the 5-membered ring of the purine

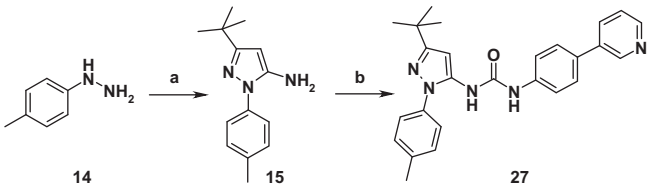

Scheme 1. Reagents and conditions: (a) Pivaloylactonitrile, toluene, 110 °C, 4 h; (b) (i) phenyl chloroformate, THF, pyridine, 0 °C to rt, 5 h, (ii) 4-pyridin-3-yl-phenylamine, DMSO, 90 °C, 12 h.

Table 1
SAR-table of optimized 5-rings

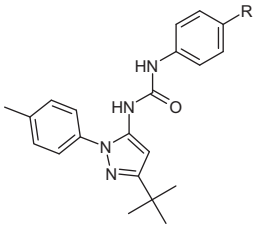

		FAK biochemical assay	FAK SPR result			HT-29[a]
Compound	R	IC_{50}[b] (μM)	K_D (μM)	k_d (s^{-1})	k_a ($M^{-1}s^{-1}$)	IC_{50} (μM)
13	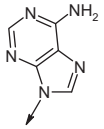	0.266	0.111	0.0007	6855	0.75
16	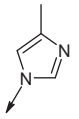	7.7	1.04	0.0017	1612	>10
17		9.1	1.53	0.0026	1706	>10
18		>10	3.12	0.0037	1175	n.d.
19	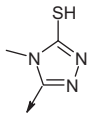	>10	4.00	0.0033	819	n.d.
20	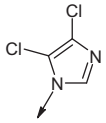	8.4	4.59	0.0014	297	>10
21		>10	9.02	0.0037	410	n.d.
22		>10	10.8	0.0038	356	n.d.
23		>10	12.4	0.0079	636	n.d.
24		>10	15.9	0.0055	348	n.d.
25		>10	17.1	0.0123	720	n.d.
26		>10	17.6	0.0037	210	n.d.

[a] Tyr397 phosphorylation of FAK in HT-29 cells (n.d. = not determined).[25]
[b] Mean of three determinations, variations about ± 5%.

scaffold of **13** contacts the hinge region by one classical H-bond to Cys502 and one non-classical H-bond to Glu500 (Fig. 3a). Differently to the binding mode of ATP, none of the 6-membered purine ring N-atoms forms direct H-bonds to the hinge region. Also, the exocyclic amine group of **13** is oriented in H-bond distance to the carbonyl O-atom of Cys502 and not of Glu500, as in the FAK-structure with ATP (Supplementary Fig. 2S). As indicated by the observed H-bond pattern, the purine ring of **13** might not be an optimal hinge-binder in combination with the phenylurea linker and the substituted pyrazole in the type II backpocket. Therefore, we inspected our fragment hits for suitable hinge binders with less molecular weight and heteroatom content as the pur-

Table 2
SAR-table of optimized 6-rings

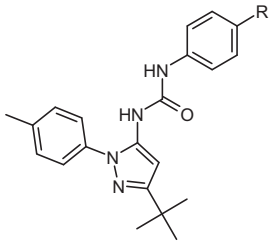

		FAK biochemical assay	FAK SPR result			HT-29 [a]
Compound	R	IC_{50}[b] (μM)	K_D (μM)	k_d (s^{-1})	k_a ($M^{-1}s^{-1}$)	IC_{50} (μM)
13	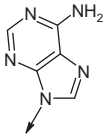	0.266	0.111	0.0007	6855	0.75
27		7.0	0.77	0.0008	1091	>10
28	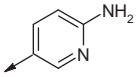	5.0	3.1	0.0008	262	n.d.
29		>10	38.8	0.0129	332	n.d.
30	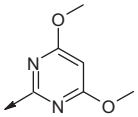	>10	9.63	0.0012	124	n.d.
31	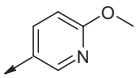	>10	>100[c]	–	–	n.d.
32	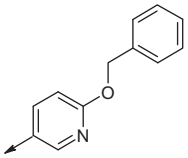	>10	>25[d]	–	–	n.d.

[a] Tyr397 phosphorylation of FAK in HT-29 cells (n.d. = not determined).[25]
[b] Mean of three determinations, variations about ± 5%.
[c] No binding observed up to a compound concentration of 100 μM.
[d] Solubility issues observed for compound concentrations >25 μM.

ine ring to also reduce the polar surface area for optimal pharmacokinetic properties.

Superimposition of the FAK crystal structures in complex with **13** and the fragment hits **3** and **6** readily engendered ideas for introducing alternative hinge-binders. The hinge binding pyrazole ring of **6** suggested purine replacement by a 5-membered ring bearing an acceptor N-atom in the 3-position to the phenylurea linker for contacting the backbone-NH donor of Cys502 (Fig. 4a). Alternatively, superimposition with fragment hit **3** led to 6-membered rings like 3-pyridine as purine surrogates to form suitable H-bonds with Cys502 (Fig. 4b). Accordingly, we prepared phenylurea substituted pyrazoles **16**–**26** and **27**–**32** (5- and 6-ring hinge-binders) in a two-step sequence starting from the commercially available *p*-tolylhydrazine **14** (Scheme 1). Synthesis of the three-fold substituted pyrazole **15**, the activation procedure via the phenyl carbamate and the preparation of ureas like **27** were conducted as described before.[3,28,29] Binding affinities measured in the biochemical FAK assay revealed significantly increased IC_{50}s of more than 20-fold for all synthesized derivatives **16**–**32** compared to the HTS-hit **13** (IC_{50} = 266 nM). Indeed, only three 5-ring analogues bearing an imidazole ring as hinge-binder showed IC_{50}s below 10 μM: **16** (IC_{50} = 7.7 μM), **17** (IC_{50} = 9.1 μM) and **20** (IC_{50} = 8.4 μM) (Table 1). However, binding was confirmed by SPR with dissociation constants in the range between 1.04 and 17.6 μM for all 5-ring analogues **16**–**26**. Both assays indicated the 4-methylimidazole derivative **16** as the most potent follow-up compound (IC_{50} = 7.7 μM, K_D = 1.04 μM). In the series of 6-ring hinge-binders, the 3-pyridine **27** was the most active analogue with submicromolar affinity (K_D = 0.77 μM) in the SPR binding assay (Table 2).

A closer analysis of binding kinetics suggests, that purine replacement in **13** by 5- or 6-rings was accompanied by a drop in association (k_a, on-rate) and by an increase in dissociation rate constants (k_d, off-rates). The on-rate of the most active 5-ring and 6-ring derivatives is reduced by factors of 4–6 (**16**: k_a = 1612 - M^{-1} s^{-1}; **27**: k_a = 1091 M^{-1} s^{-1}) compared to **13** (k_a = 6855 M^{-1} - s^{-1}). However, the off-rates of **16** (k_d = 0.0017 s^{-1}) and **27** (k_d = 0.0008 s^{-1}) are already in a similar range as for **13** (k_d = 0.0007 s^{-1}) indicating a slow release of the deeply buried inhibitor from the protein as reported for other type II binders.[30] Indeed, the X-ray structure of FAK in complex with **27** confirmed the type II binding mode as observed for **13** as well as the designed

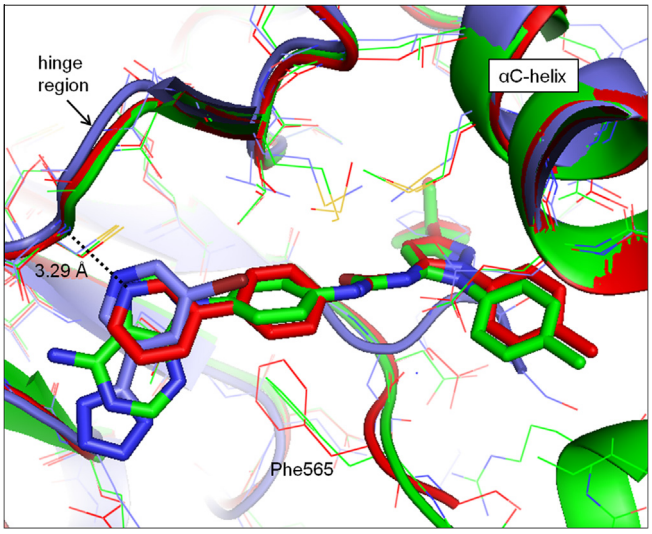

Figure 5. Comparison of FAK X-ray structures with the original type II binder **13** (green), fragment hit **3** (blue) and the designed follow-up inhibitor **27** (red, PDB ID: 4KAO). Fragment-merging maintained a type II binding conformation of **27** with 3-pyridine as suitable purine replacement for H-bond interaction (dotted line) to the hinge region.

H-bond of the 3-pyridine ring towards the backbone-NH of Cys502 (Fig. 5). A prolonged residence time has been proposed as useful parameter in the context of compound optimization towards cellular and in vivo efficacy.[31,32] In our previous structure-based optimization study of fragment hit **5** we concluded, that off-rates below 0.01 s^{-1} seem to be necessary for achieving submicromolar inhibition of FAK autophosphorylation at Tyr397 in HT-29 cells.[24] However, cellular activity was observed only for the initial HTS-hit **13** (P-Tyr397-FAK (HT-29) IC_{50} = 0.75 μM), but not for the 5- and 6-ring derivatives **16** and **27** (P-Tyr397-FAK (HT-29) IC_{50} >10 μM) despite their low off-rates below 0.01 s^{-1}.[25] Therefore, a low off-rate alone might not be sufficient for cellular activity and additional properties such as target potency, cell permeability or plasma protein binding need to be further optimized.

As first guidelines for ADME fine tuning, we have analyzed relevant experimental physicochemical parameters such as solubility, log*D*, log *P* and the in vitro clearance (Cl_{int}) of our series (Table 3). The log*D*-values of the series analogues are not very different in the range between 3.2 and 4.6 and might be further diminished to achieve permeable and metabolic stable compounds (log*D* range of 1.0–2.0).[33] Reduction of the polar surface area is often beneficial in the optimization of compound properties including cellular potency and intestinal permeability.[34] Indeed, the topological polar surface area (tPSA) was reduced in most 5- and 6-ring analogues bearing hinge-binders with less H-bond acceptor and donor atoms (Table 3).[35,36] The decreased polarity had no adverse effect on aqueous solubility (S), which was even slightly improved in several potent 5- and 6-ring derivatives such as **17** (*S* = 23.1 μM) or **28** (*S* = 39.2 μM) in comparison to the HTS-hit **13** (*S* = 7.1 μM). Classification bands of the in vitro clearance (Cl_{int}) in liver microsomes were used to categorise compounds into low, medium or high clearance.[37–39] The HTS-hit **13** revealed high Cl_{int}-values in human and mouse liver microsomes (202 and 87 μL/min/mg). The in vitro clearance of the most active 5- and 6-ring derivatives **16**, **17** and **27** was reduced and analogues such as **23**–**25** can already be classified as medium clearance compounds with human Cl_{int} values below 50 μL/min/mg. However, the clearance need to be further reduced (<10 μL/min/mg) in order to allow first in vivo efficacy evaluation in mouse. In addition, the high plasma protein binding of the HTS-hit and analogues might also be still in a suboptimal range as indicated by low fraction unbound values (fub) <1% (Table 3). Regarding metabolic stability, most series ana-

Table 3
Physicochemical properties and in vitro ADME parameters

Compd	Solubility[a] (μM)	HBA[b]	HBD[b]	Log*D* pH 7.4[c]	Log*P*[d]	tPSA[e] (Å^2)	Microsomal stability,[f] Cl_{int} (μL/min/mg)		Serum protein binding,[g] fub (%)		CYP IC_{50}[h] (μM)
							Human	Mouse	Human	Mouse	
13	7.1	10	3	4.05	3.98	129	202	87	0.1	1	>10
16	4.7	7	2	4.08	4.83	77	85	75	0.06	0.1	>10
17	23.1	7	2	3.85	4.35	77	58	44	0.07	0.37	[i]
18	48.5	8	2	3.94	4.07	90	98	29	0.1	0.54	[j]
19	49.6	8	2	3.89	2.86	129	455	124	0.35	0.3	[k]
20	16.9	7	2	3.96	>5.4	77	91	114	<0.01	<0.01	>10
21	14.1	7	2	4.33	4.60	77	119	85	0.88	0.66	>10
22	15.2	7	2	4.58	5.15	85	146	197	0.06	0.08	>10
23	48.2	9	2	3.81	3.86	103	46	60	0.88	0.69	>10
24	18.2	7	2	4.49	4.96	85	46	36	0.05	0.14	>10
25	45.4	9	2	3.79	4.14	103	26	36	0.19	0.47	>10
26	89.8	8	2	3.21	3.34	90	64	31	2	1.2	>10
27	9.3	6	2	4.25	4.84	98	121	96	0.04	0.06	>10
28	39.2	7	3	3.88	5.13	72	97	83	n.d.	n.d.	>10
29	15.2	6	2	3.58	>5	72	104	53	<0.1	<0.1	>10
30	4.9	9	2	3.94	>5.4	103	28	43	n.d.	n.d.	>10
31	2.8	7	2	4.02	4.25	81	n.d.	n.d.	n.d.	n.d.	>10
32	9.3	7	2	3.94	>5.4	81	101	65	n.d.	n.d.	>10

[a] The kinetic solubility was measured in phosphate buffer at pH 7.4 by HPLC.
[b] Number of H-bond acceptors (HBA) and H-bond donors (HBD) calculated with MOE.[36]
[c] Measured log*D* at pH 7.4.
[d] Measured log*P*.
[e] The topological surface area (tPSA) was calculated with MOE.[36]
[f] The in vitro clearance was measured in human and mouse liver microsomes (n.d. = not determined).
[g] Serum protein binding (fub = fraction unbound).
[h] Cyp assay versus 1A2, 2C8, 2C9, 2C19, 2D6, and 3A4.
[i] Cyp IC_{50}s of 0.4, 0.8 and 0.4 μM versus 2C8, 2C9 and 2D6.
[j] Cyp IC_{50}s of 6.9 and 5 μM versus 2C9 and 2D6.
[k] Cyp IC_{50} of 4.8 μM versus 2D6.

logues showed no cytochrome P-450 (CYP) inhibition below 10 μM with the exception of the imidazole derivative **17** (Table 3). The introduction of additional lipophilic substituents into the core structure might be limited based on log*P*-values around 5 for most analogues. Structure-based design guided by our FAK-fragment X-ray structures might identify positions in our 5- and 6-ring analogues for adding at least one specific H-bond to also improve the on-rates of binding.

Finally, we monitored the impact of exchanging the purine hinge-binder of **13** by measuring kinase selectivity in comparison with the 5- and 6-ring derivatives **16** and **27**. The compounds were tested in a panel of 48 protein kinases using a radioactive filter-binding assay resulting in the inhibition of 14 kinases with <−50% effect at 1 μM for **13** and smaller portions for **16** (6 out of 48) and **27** (7 out of 45, Supplementary Table S2). These data give only a first estimate of selectivity, since they are not based on IC_{50}s and limited to only 10% of the kinome. Also, the FAK affinities based on the $K_{d,ss}$-values for **16** and **27** are 10- and 7-fold lower compared to **13**.

In summary, we have identified a significant number of alternative hinge-binders for FAK by SPR and elucidated their detailed binding mode by protein crystallography. Fragment-merging by combining suitable 5- and 6-membered hinge-binders with a type II inhibitor discovered by HTS resulted in follow-up compounds with comparable off-rates, but reduced binding affinity. The large variety of identified fragments bound to the ATP-site of FAK together with the type II inhibitor will further guide our hit-optimization efforts to increase the on-rate to achieve suitable cellular potency. Fragment-growing might be used to exploit potential alternatives of the urea moiety facilitating the type II conformation to further enhance kinase selectivity.

Supplementary data

Supplementary data associated with this article can be found, in the online version, at http://dx.doi.org/10.1016/j.bmcl.2013.07.050.

References and notes

1. Hall, J. E.; Fu, W.; Schaller, M. D. *Int. Rev. Cell Mol. Biol.* **2011**, *288*, 185.
2. Peng, X.; Guan, J. L. *Curr. Protein Pept. Sci.* **2011**, *12*, 52.
3. Bagley, M. C.; Davis, T.; Dix, M. C.; Widdowson, C. S.; Kipling, D. *Org. Biomol. Chem.* **2006**, *4*, 4158.
4. Lietha, D.; Cai, X.; Ceccarelli, D. F.; Li, Y.; Schaller, M. D.; Eck, M. J. *Cell* **2007**, *129*, 1177.
5. Cance, W. G.; Harris, J. E.; Iacocca, M. V.; Roche, E.; Yang, X.; Chang, J.; Simkins, S.; Xu, L. *Clin. Cancer Res.* **2000**, *6*, 2417.
6. Golubovskaya, V. M.; Kweh, F. A.; Cance, W. G. *Histol. Histopathol.* **2009**, *24*, 503.
7. McLean, G. W.; Carragher, N. O.; Avizienyte, E.; Evans, J.; Brunton, V. G.; Frame, M. C. *Nat. Rev. Cancer* **2005**, *5*, 505.
8. Hennig, M.; Ruf, A.; Huber, W. *Top. Curr. Chem.* **2012**, *317*, 115.
9. Lepre, C. A. *Methods Enzymol.* **2011**, *493*, 219.
10. Scott, D. E.; Coyne, A. G.; Hudson, S. A.; Abell, C. *Biochemistry* **2012**, *51*, 4990.
11. Fragment criteria include: MW <250; calculated solubility ($c\log S$)>−3; number of hydrogen bond donors (<4) and acceptors (<6).
12. *SPR*. The kinase domain of FAK was immobilized in the presence of an ATP site-specific Inhibitor onto CM5 (series S) sensor chips using standard amine coupling. FAK inhibitor compounds (stored as 10 mM stock solutions in 100% DMSO) were diluted in running buffer (10 mM HEPES, 150 mM NaCl, 5 mM $MgCl_2$, 1 mM DTT, 0.05% Tween20, and 2% DMSO, pH 7.4) and analyzed with a Biacore 4000 or Biacore S51 (Biacore AB, GE Healthcare Life Sciences, Uppsala, Sweden) using a 2-fold dilution series. The highest compound concentration varied according to the expected dissociation constant, but all compounds were tested at 10 different concentrations. Interaction analysis cycles were run at 30 μL/min and consisted of a 180 s sample injection followed by 240 s of buffer flow (dissociation phase). All sensorgrams were evaluated by first subtracting the binding response recorded from the control surface (reference spot), followed by subtracting a buffer blank injection. To determine kinetic rate constants, data sets were fitted to a simple 1:1 interaction model including a term for mass transport using numerical integration and nonlinear curve fitting. Equilibrium analysis was performed by fitting the response at the end of the association phase to a single-site binding isotherm.
13. Roberts, W. G.; Ung, E.; Whalen, P.; Cooper, B.; Hulford, C.; Autry, C.; Richter, D.; Emerson, E.; Lin, J.; Kath, J.; Coleman, K.; Yao, L.; Martinez-Alsina, L.; Lorenzen, M.; Berliner, M.; Luzzio, M.; Patel, N.; Schmitt, E.; LaGreca, S.; Jani, J.; Wessel, M.; Marr, E.; Griffor, M.; Vajdos, F. *Cancer Res.* **1935**, *2008*, 68.
14. *Criteria for 'category A' hits*: The SPR data matched to an 1:1 model and the compounds run into (or almost into) surface saturation without exceeding an 1:1 stoichiometry. The compound binding was blocked by the active site specific inhibitor and K_D values were averaged over two surfaces with different protein densities.
15. Bemis, G. W.; Murcko, M. A. *J. Med. Chem.* **1996**, *39*, 2887.
16. Hopkins, A. L.; Groom, C. R.; Alex, A. *Drug Discovery Today* **2004**, *9*, 430.
17. FAK protein crystallization has been performed as previously described Heinrich et al *J. Med. Chem.* **2013**, *56*, 1160.
18. Zhang, J.; Yang, P. L.; Gray, N. S. *Nat. Rev. Cancer* **2009**, *9*, 28.
19. de Kloe, G. E.; Bailey, D.; Leurs, R.; de Esch, I. J. *Drug Discovery Today* **2009**, *14*, 630.
20. Murray, C. W.; Verdonk, M. L.; Rees, D. C. *Trends Pharmacol. Sci.* **2012**, *33*, 224.
21. The atomic coordinates and structure factors for the kinase domain of FAK in complex with **3**, **6**, **13** and **27** have been deposited in the Protein Data Bank (www.rcsb.org) under the accession codes 4K8A, 4KAB, 4K9Y and 4KAO, respectively.
22. Norman, R. A.; Toader, D.; Ferguson, A. D. *Trends Pharmacol. Sci.* **2012**, *33*, 273.
23. Iwatani, M.; Iwata, H.; Okabe, A.; Skene, R. J.; Tomita, N.; Hayashi, Y.; Aramaki, Y.; Hosfield, D. J.; Hori, A.; Baba, A.; Miki, H. *Eur.J. Med. Chem.* **2012**, *61*, 60.
24. Heinrich, T.; Seenisamy, J.; Emmanuvel, L.; Kulkarni, S. S.; Bomke, J.; Rohdich, F.; Greiner, H.; Esdar, C.; Krier, M.; Gradler, U.; Musil, D. *J.Med. Chem.* **2013**, *56*, 1170.
25. *FAK-kinase assay (autophosphorylation)*. The FAK assay is performed as a 384-well Flashplate assay. A 2 nM concentration of FAK, 400 nM biotinylated substrate [His-TEVhsFAK(31−686)(K454R) × Biotin], and 1 μM ATP (spiked with 0.25 μCi ^{33}P-ATP/well) are incubated in a total volume of 50 μL [60 mM 4-(2-hydroxyethyl)-1-piperazineethanesulfonic acid (HEPES), 10 mM $MgCl_2$, 1.2 mM dithiothreitol, 0.02% Brij35, 0.1% BSA, pH 7.5] with or without test compound for 2 h at 30 °C. The reaction was stopped with 25 μL of 200 mM EDTA. After 30 min at 30 °C, the liquid was removed, and each well waswashed thrice with 100 μL of 0.9% sodium chloride solution. A nonspecific reaction was determined in the presence of 1 μM PF-431396. Radioactivity was measured with a Topcount Microplate Scintillation Counter (Perkin–Elmer). Results were calculated with Symyx Assay Explorer. *P-Y397-FAK cellular assay*. HT29 cells that have gene amplification of FAK were plated at 30,000 cells/well in a 96-well microtiter plate and allowed to adhere overnight. Inhibitor compounds were added to each well in a threefold serial dilution (range from 0.03 to 30 μM) in triplicate for 45 min. After compound treatment, cells were lysed and cleared by centrifugation through a 96-well filter plate. FAK was captured from total lysates by incubation with a mouse-anti-FAK antibody (Merck Millipore, #05-537) coupled to Luminex microspheres overnight. The level of P-Y397-FAK was then detected by applying a rabbit-anti-P-Y397-FAK antibody (Sigma, #F7926) and an antirabbit-PE secondary antibody in a Luminex100 machine according to the manufacturer's instructions. Samples treated with dimethylsulfoxide (DMSO) vehicle were set as maximal phosphorylation, and inhibitor-treated samples were calculated as the percent inhibition. Nonlinear regression analysis (variable slope) was applied for the determination of IC_{50} values (Accelry Assay Explorer).
26. Han, S.; Mistry, A.; Chang, J. S.; Cunningham, D.; Griffor, M.; Bonnette, P. C.; Wang, H.; Chrunyk, B. A.; Aspnes, G. E.; Walker, D. P.; Brosius, A. D.; Buckbinder, L. *J. Biol. Chem.* **2009**, *284*, 13193.
27. Avraham, H.; Park, S. Y.; Schinkmann, K.; Avraham, S. *Cell. Signal.* **2000**, *12*, 123.
28. Moss, N.; Breitfelder, S.; Betageri, R.; Cirillo, P. F.; Fadra, T.; Hickey, E. R.; Kirrane, T.; Kroe, R. R.; Madwed, J.; Nelson, R. M.; Pargellis, C. A.; Qian, K. C.; Regan, J.; Swinamer, A.; Torcellini, C. *Bioorg. Med. Chem. Lett.* **2007**, *17*, 4242.
29. Suijkerbuijk, B. M.; Niculescu-Duvaz, I.; Gaulon, C.; Dijkstra, H. P.; Niculescu-Duvaz, D.; Menard, D.; Zambon, A.; Nourry, A.; Davies, L.; Manne, H. A.; Friedlos, F.; Ogilvie, L. M.; Hedley, D.; Lopes, F.; Preece, N. P.; Moreno-Farre, J.; Raynaud, F. I.; Kirk, R.; Whittaker, S.; Marais, R.; Springer, C. J. *J. Med. Chem.* **2010**, *53*, 2741.
30. Iwata, H.; Imamura, S.; Hori, A.; Hixon, M. S.; Kimura, H.; Miki, H. *Biochemistry* **2011**, *50*, 738.
31. Copeland, R. A.; Pompliano, D. L.; Meek, T. D. *Nat. Rev. Drug Disc.* **2006**, *5*, 730.
32. Lu, H.; Tonge, P. J. *Curr. Opin. Chem. Biol.* **2010**, *14*, 467.
33. Johnson, T. W.; Dress, K. R.; Edwards, M. *Bioorg. Med. Chem. Lett.* **2009**, *19*, 5560.
34. Clark, D. E. *Future Med. Chem.* **2011**, *3*, 469.
35. Ertl, P.; Rohde, B.; Selzer, P. *J. Med. Chem.* **2000**, *43*, 3714.
36. Molecular Operating Environment (MOE), 2. 1.; Chemical Computing Group Inc., 1. S. St. W. S. #. M. Q. C. H. 2. 2, In: 2013.
37. Barter, Z. E.; Bayliss, M. K.; Beaune, P. H.; Boobis, A. R.; Carlile, D. J.; Edwards, R. J.; Houston, J. B.; Lake, B. G.; Lipscomb, J. C.; Pelkonen, O. R.; Tucker, G. T.; Rostami-Hodjegan, A. *Curr. Drug Metab.* **2007**, *8*, 33.
38. Davies, B.; Morris, T. *Pharm. Res.* **1993**, *10*, 1093.
39. Iwatsubo, T.; Suzuki, H.; Sugiyama, Y. *J. Pharmacol. Exp. Ther.* **1997**, *283*, 462.